Supplement of The Cryosphere, 20, 5345–5363, 2026
https://doi.org/10.5194/tc-20-5345-2026-supplement

The Cryosphere
Open Access

Supplement of

Parameterizing tidal-water intrusions in long-term Antarctic ice-sheet projections

Antonio Juarez-Martinez et al.

Correspondence to: Antonio Juarez-Martinez (antjua01@ucm.es)

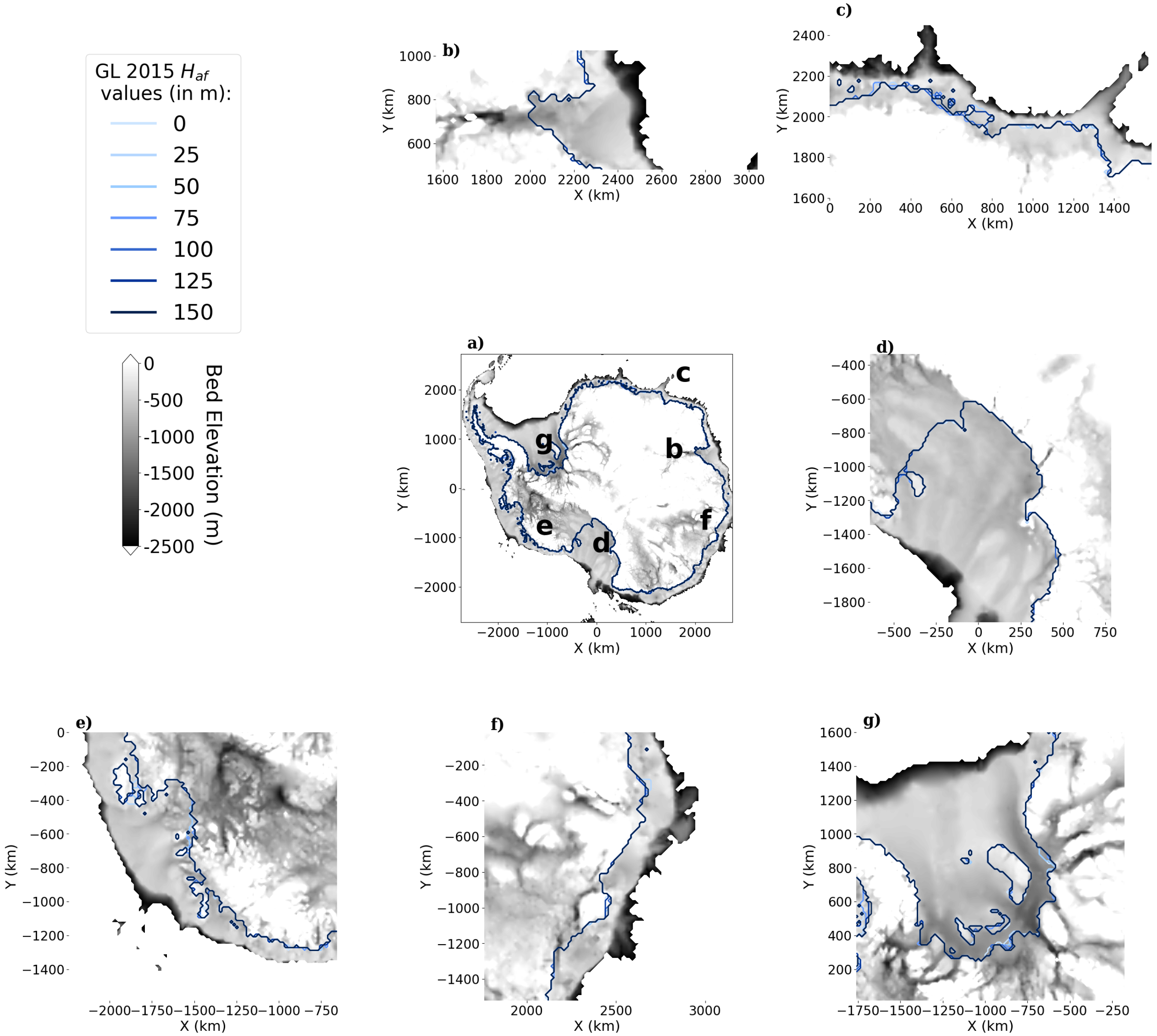

Figure S1. Grounding-line position (defined as $H_{\mathrm{af}} = 0$) at the beginning of the projections for the different values of H_t used in the spinup runs. For the different subplots, particular regions of the AIS (a) have been zoomed in: b) Amery, c) Queen Maud Land, d) Ross Ice Shelf, e) Amundsen Sea Embayment, f) Wilkes Land and g) Ronne-Filchner Ice Shelf.

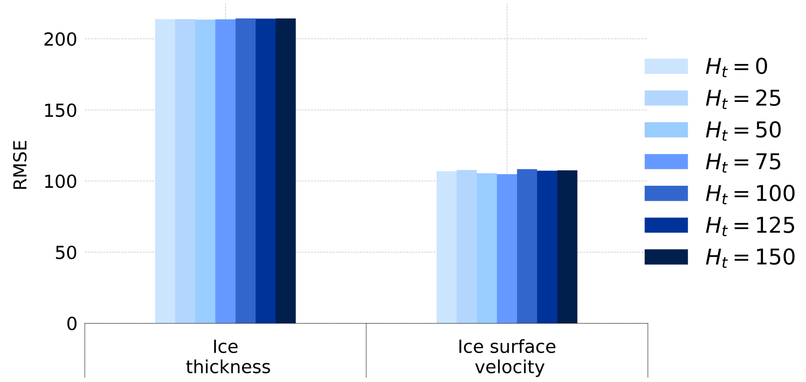

Figure S2. Root-mean-square error (RMSE) for ice thickness (in m) and ice-surface velocity (in $\mathrm{m\,yr^{-1}}$) between the start of the simulations in 2015 and observations from the Bedmap3 (Pritchard et al., 2025) and the Rignot et al. (2011) datasets, respectively. The different colours represent different values of H_t.

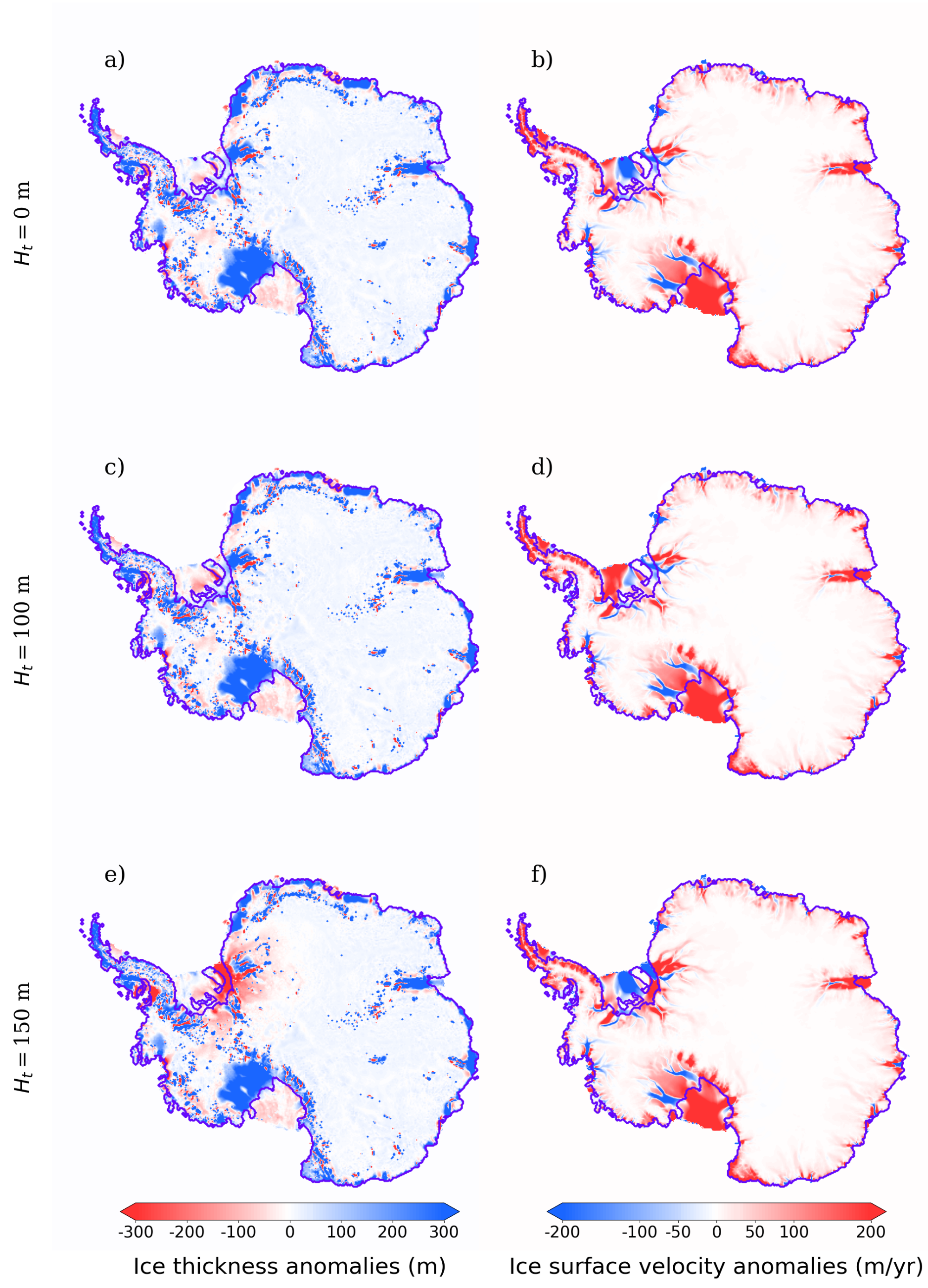

Figure S3. Errors in simulated ice thickness (in m) and surface velocity (in $\mathrm{m\,yr^{-1}}$) at the end of the spinup for $H_t = 0$ m (a,b), $H_t = 100$ m (c,d) and $H_t = 150$ m (e,f), calculated as anomalies with respect to the Bedmap3 dataset (Pritchard et al., 2025) and the Rignot et al. (2011) dataset, respectively. In purple, GL defined as $H_{\mathrm{af}} = 0$.

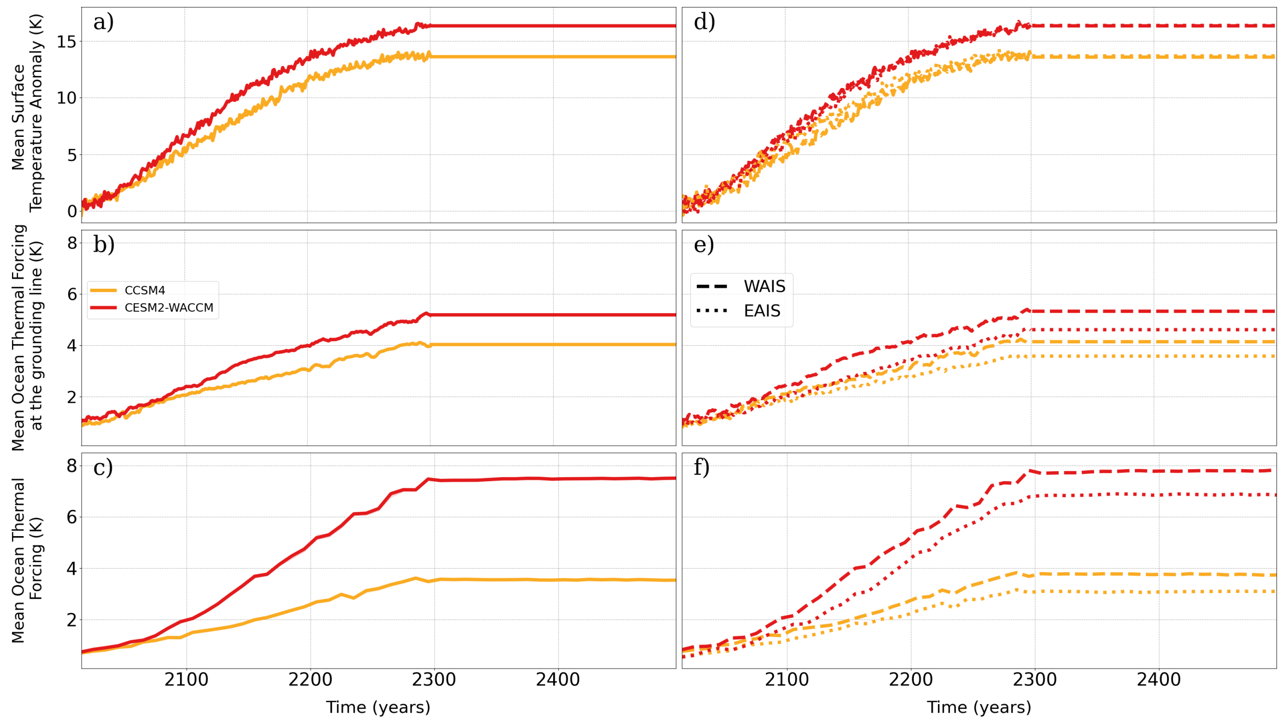

Figure S4. Mean evolution of the atmospheric (a), oceanic thermal forcing at the GL depth fixed in 2015 (b) and thermal forcing at the evolving GLs (c) in the AIS for CESM2-WACCM (SSP5-8.5) and CCSM4 (RCP8.5) until year 2500. For (d), (e) and (f), same as in (a), (b) and (c), respectively, but for the WAIS and EAIS (modified from Juarez-Martinez et al., 2024).

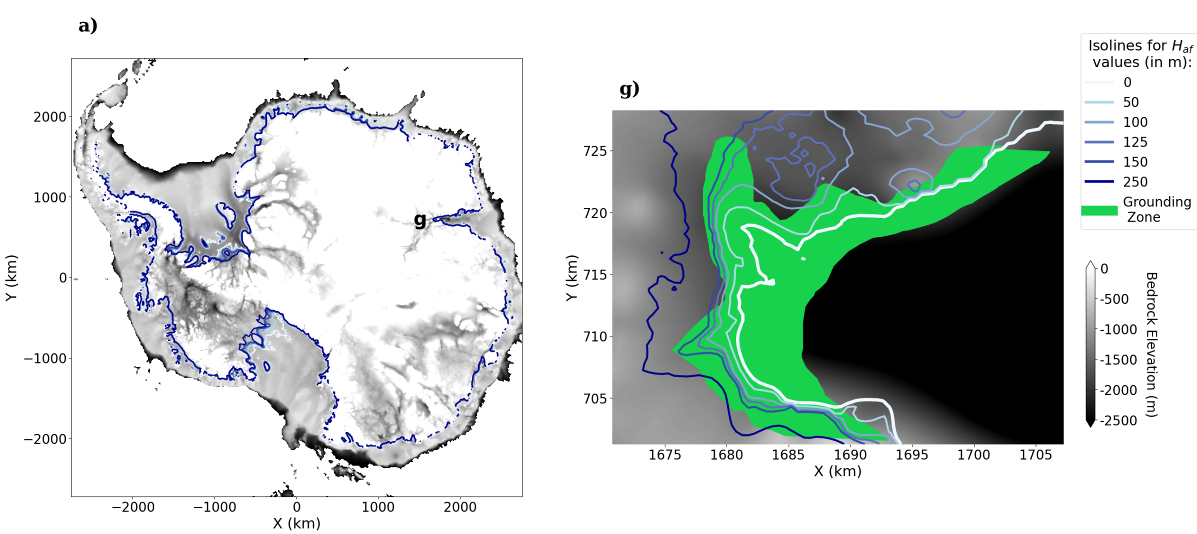

Figure S5. Same as Figure 2f, but considering the western most region of the Amery Ice Shelf (Chen et al., 2023). The mean and median values are -39.0 m and 21.7 m, respectively.

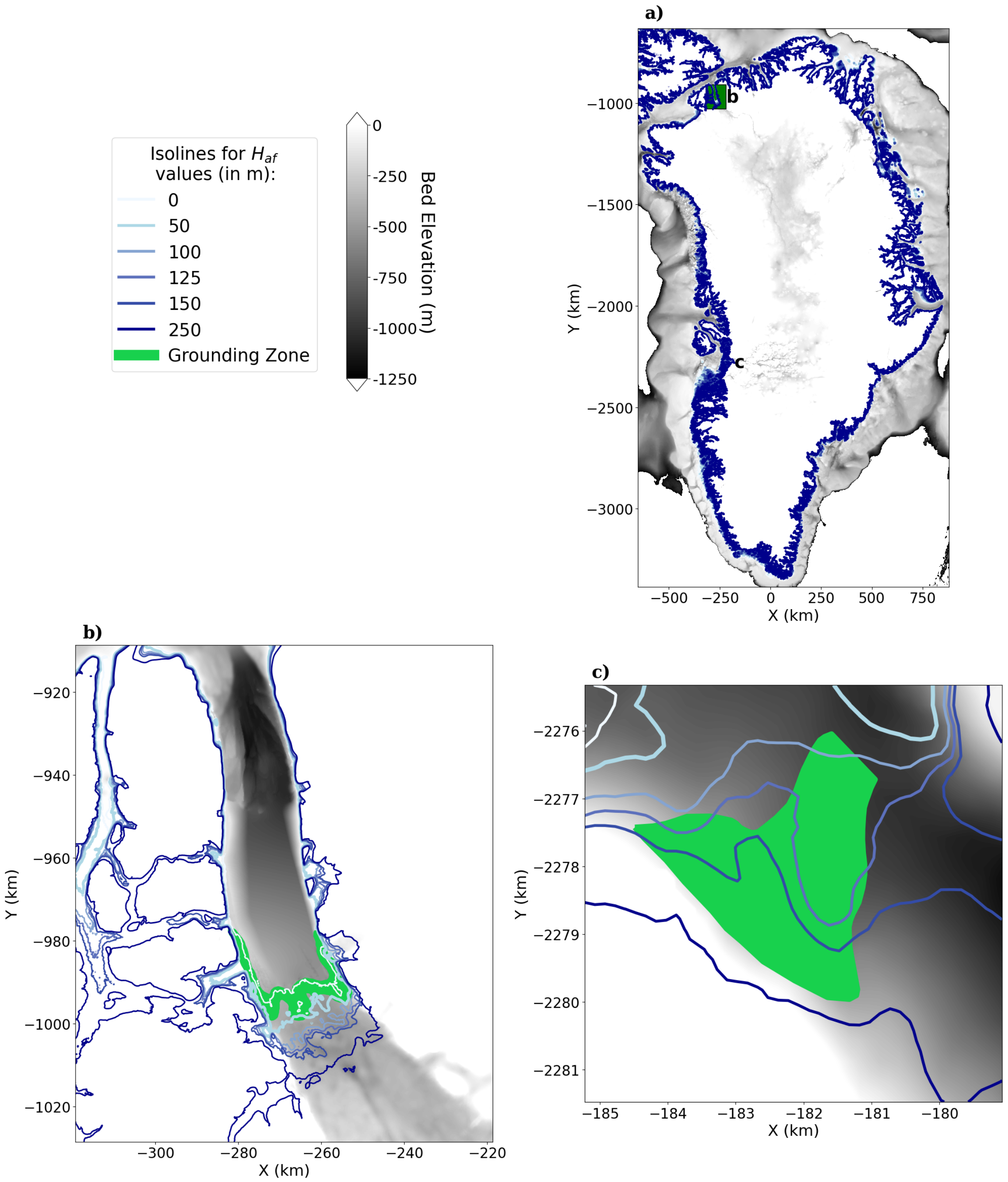

Figure S6. a) Observational estimates of two GZ for different regions in Greenland compared with isolines of thickness above flotation. Rectangles with letters b-c delimit the extension of the different regions of the insets, for which the observational GZ obtained through DInSAR from different studies is shown in green, b) Petermann Glacier (Ciracì et al., 2023) and c) Jakobshavn Isbræ (Kim et al., 2024). Bathymetric dataset used from BedMachine Greenland V5 (Morlighem et al., 2022) with a resolution of 150 m.

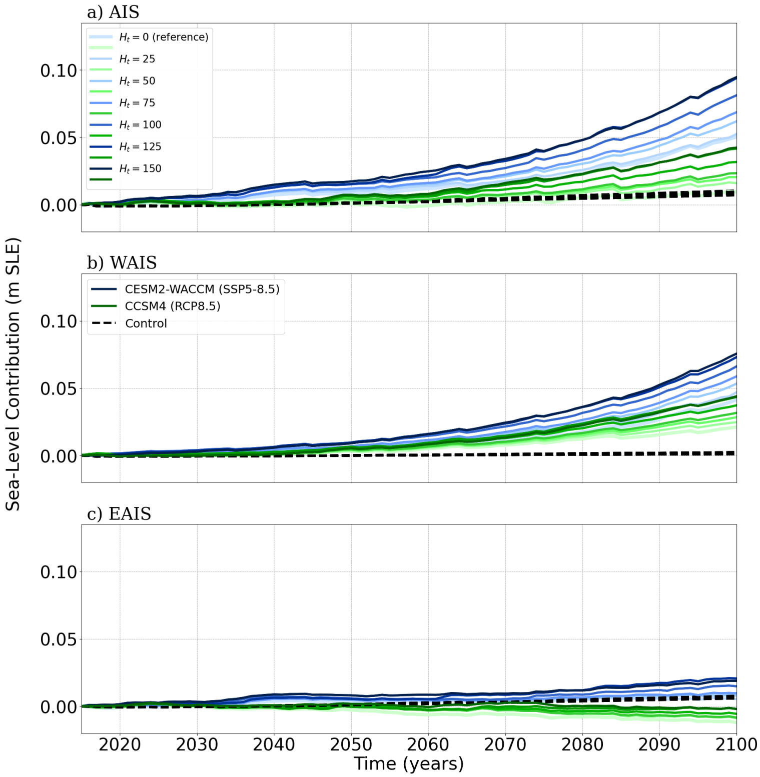

Figure S7. As Figure 3, but until 2100.

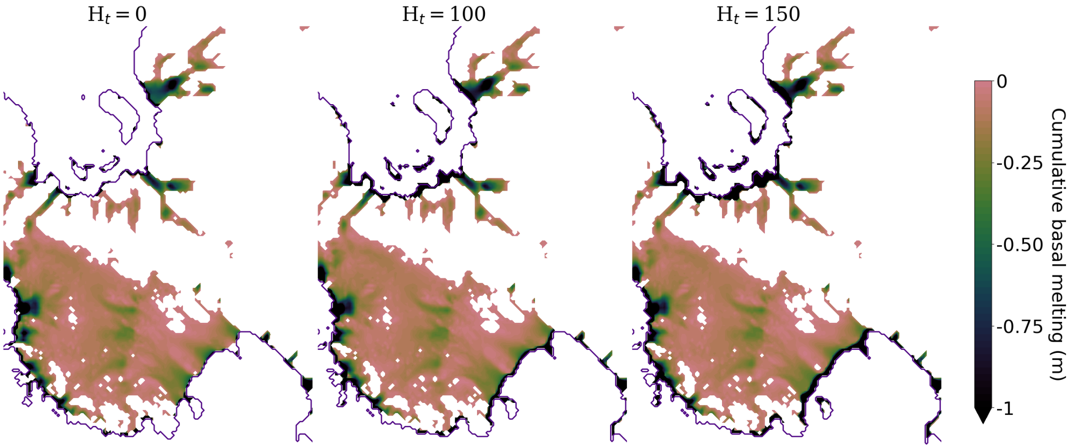

Figure S8. Zoom-in (in the WAIS) of cumulative basal mass balance w.r.t control at the initial time (m) until 2025 for different H_t values for CESM2-WACCM (SSP5-8.5). GL as defined by $H_{\mathrm{af}} = 0$ is shown in purple in order to better identify the area. Positive values have been masked.

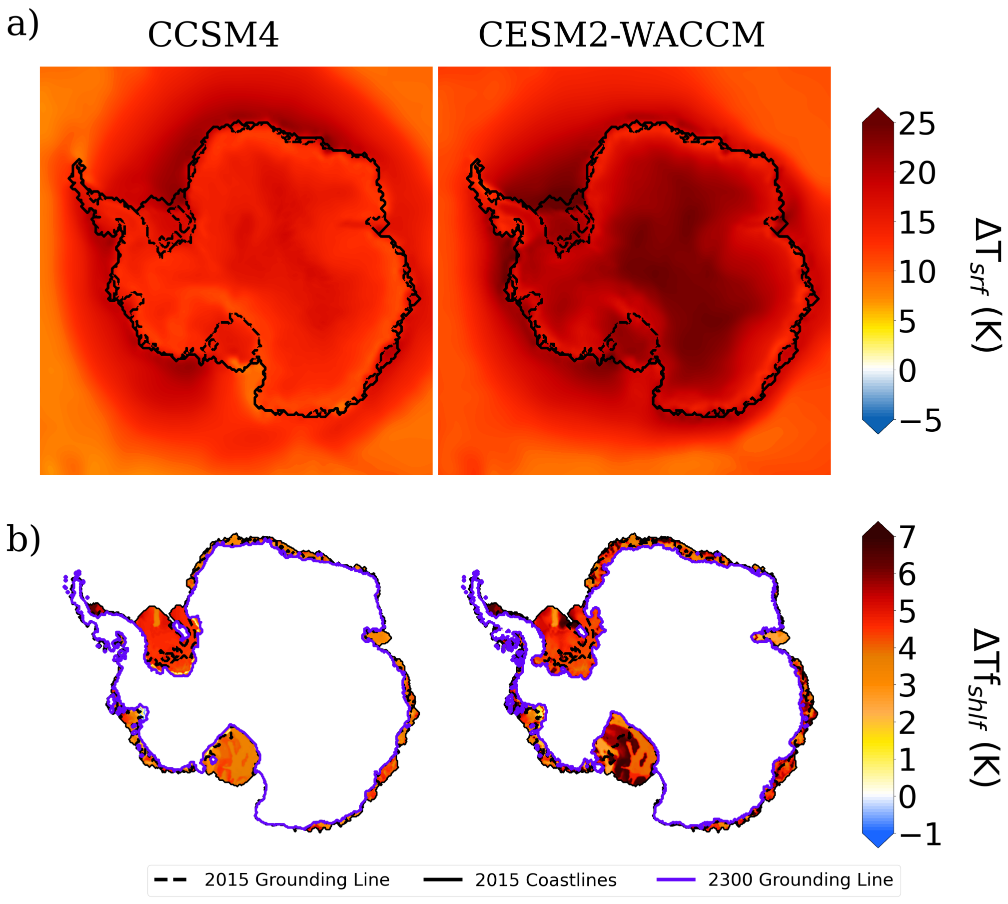

Figure S9. Anomalies in a) surface temperature (K) and b) thermal forcing (K) between 2300 and 2015 for CCSM4 (RCP8.5) and CESM2-WACCM (SSP5-8.5) (modified from Juarez-Martinez et al., 2024).

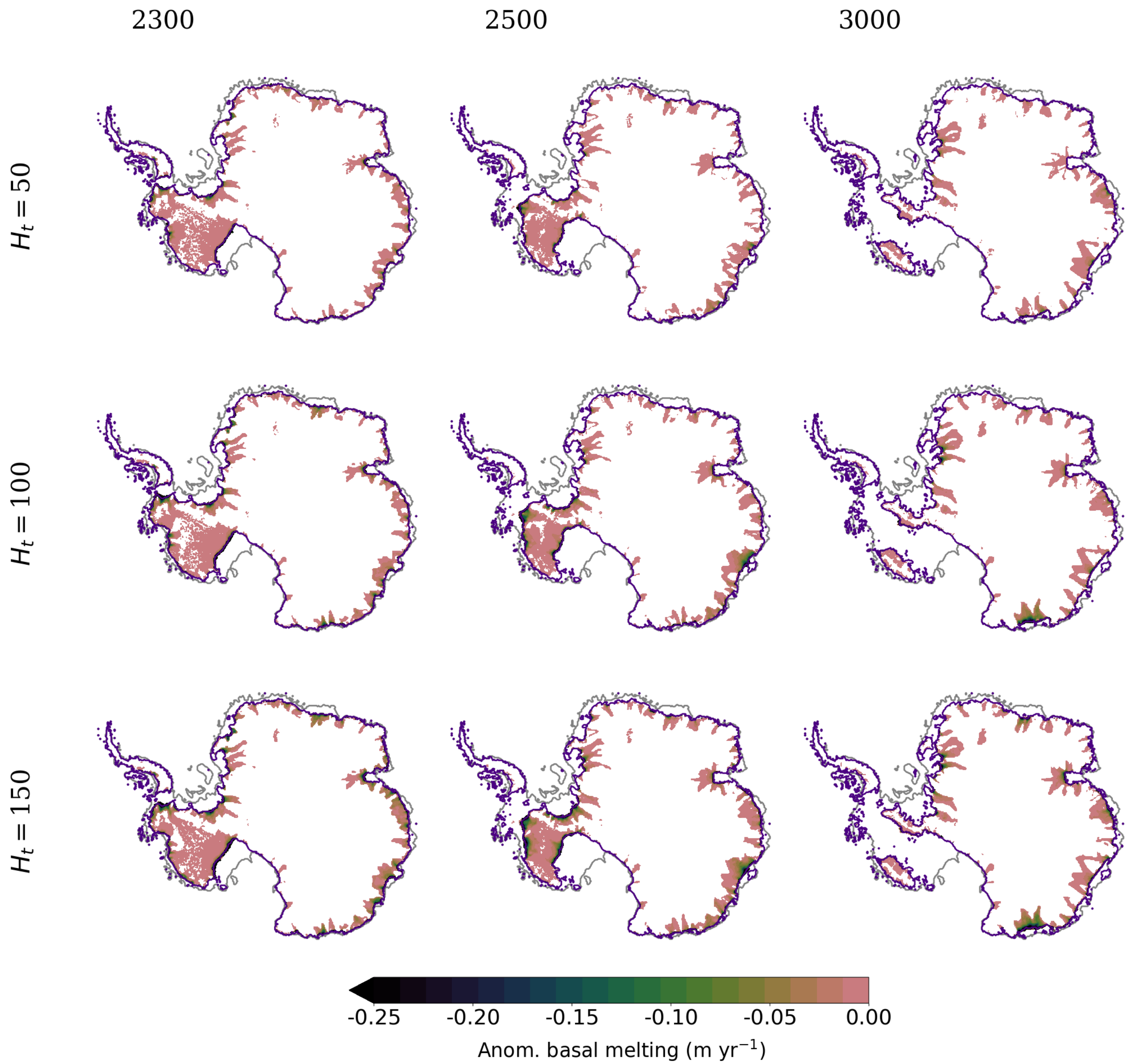

Figure S10. Basal melting anomalies ($\mathrm{m\,yr^{-1}}$) for the different values of H_t at different timesteps with respect to the case where $H_t = 0$ m for the experiments with CESM2-WACCM (SSP5-8.5). The gray and purple lines represent the initial and evolving GL, respectively (defined as $H_{\mathrm{af}} = 0$).

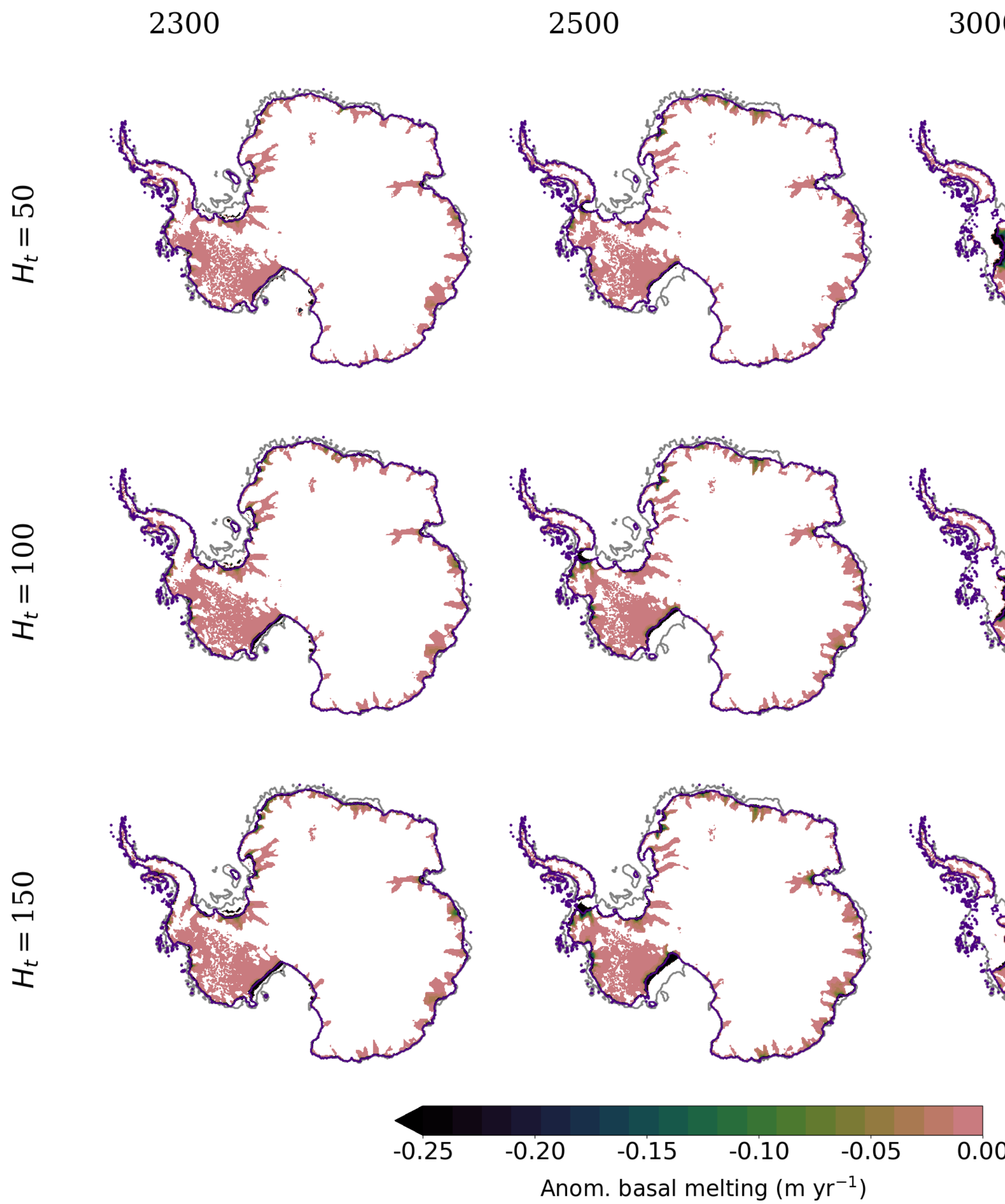

Figure S11. Same as Figure S10, but for the experiments with CCSM4 (RCP8.5).

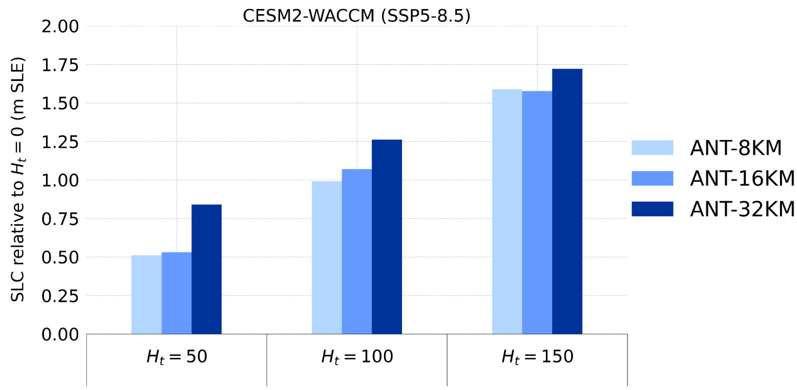

Figure S12. Sea-level contribution relative to $H_t = 0$ (m SLE) at year 3000 for the three resolutions, 8, 16 and 32 km, using different values of H_t, under the CESM2-WACCM (SSP5-8.5) climate forcing.

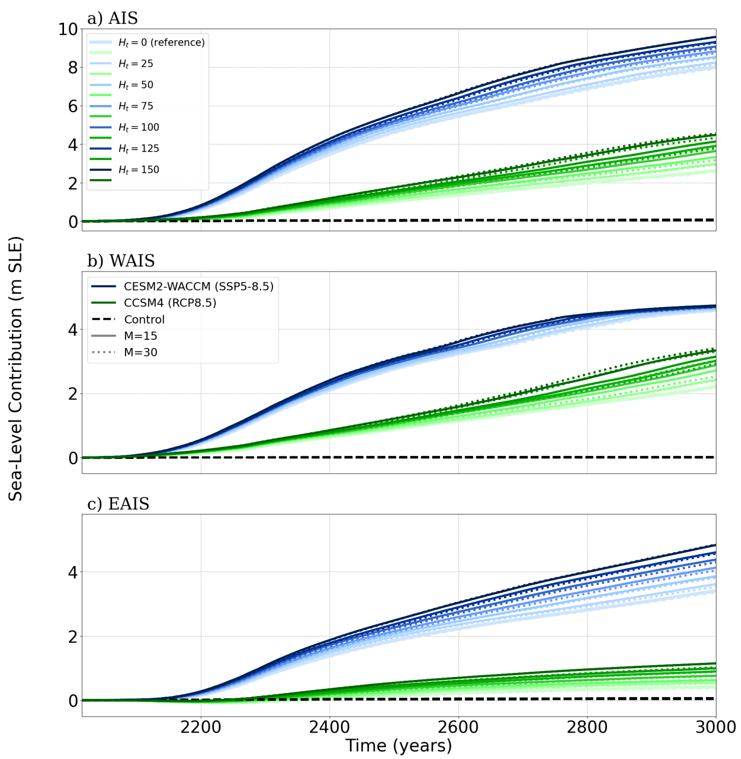

Figure S13. Sea-level contribution (m SLE) using two different values of the parameter M in the PMPT parameterization, for the two climatic forcings: CESM2-WACCM (SSP5-8.5) and CCSM4 (RCP8.5).

References

Chen, H., Rignot, E., Scheuchl, B., and Ehrenfeucht, S.: Grounding zone of Amery ice shelf, Antarctica, from differential synthetic-aperture radar interferometry, Geophysical Research Letters, 50, e2022GL102 430, https://doi.org/10.1029/2022GL102430, 2023.

Ciracì, E., Rignot, E., Scheuchl, B., Tolpekin, V., Wollersheim, M., An, L., Milillo, P., Bueso-Bello, J.-L., Rizzoli, P., and Dini, L.: Melt rates in the kilometer-size grounding zone of Petermann Glacier, Greenland, before and during a retreat, Proceedings of the National Academy of Sciences, 120, e2220924 120, https://doi.org/10.1073/pnas.2220924120, 2023.

Juarez-Martinez, A., Blasco Navarro, J., Robinson, A., Montoya, M., and Alvarez-Solas, J.: Antarctic sensitivity to oceanic melting parameterizations, The Cryosphere, 18, 4257–4283, https://doi.org/10.5194/tc-18-4257-2024, 2024.

Kim, J., Rignot, E., Holland, D., and Holland, D.: Seawater Intrusion at the Grounding Line of Jakobshavn Isbræ, Greenland, From Terrestrial Radar Interferometry, Geophysical Research Letters, 51, https://doi.org/10.1029/2023GL106181, 2024.

Morlighem, M. et al.: IceBridge BedMachine Greenland, Version 5, https://doi.org/10.5067/GMEVBWFLWA7X, 2022.

Pritchard, H., Fretwell, P., Fremand, A., Bodart, J., Kirkham, J., Aitken, A., Bamber, J., Bell, R., Bianchi, C., Bingham, R. G., Blankenship, D., Casassa, G., Christianson, K., Conway, H., Corr, H., Xiangbin, C., Damaske, D., Damm, V., Dorschel, B., and Zirizzotti, A.: Bedmap3 updated ice bed, surface and thickness gridded datasets for Antarctica, Scientific Data, 12, https://doi.org/10.1038/s41597-025-04672-y, 2025.

Rignot, E., Mouginot, J., and Scheuchl, B.: Antarctic Grounding Line Mapping from Differential Satellite Radar Interferometry, Geophys. Res. Lett., 38, https://doi.org/10.1029/2011GL047109, 2011.